

# Deformation Mechanisms in Nanotwinned Tungsten Nanopillars: Effects of Coherent Twin Boundary Spacing

Shuozhi Xu,\* Saeed Zare Chavoshi, and Yanqing Su

Nano-scale coherent twin boundaries (CTBs) significantly alter the mechanical and electrical properties of metallic materials. Despite a number of studies of the nanotwinned nanopillars in face-centered cubic metals, investigations of them in body-centered cubic (BCC) systems are rare. In this Letter, we explore the uniaxial deformation mechanisms of BCC tungsten nanopillars containing nano-scale  $\{112\}$  CTBs using molecular dynamics (MD) simulations. Our work reveals a novel tension–compression asymmetric stress–strain response and deformation behavior, in conjunction with the effects of CTB spacing. With a relatively large CTB spacing, the plastic deformation in nanotwinned nanopillars is mainly controlled by dislocation nucleation from surface/CTB intersections, gliding on distant and adjacent slip planes under tensile and compressive loading, respectively; as a result, the tensile yield stress is almost invariant with respect to the CTB spacing, while the compressive yield stress increases with a decreasing CTB spacing. As the CTB spacing reduces to 1 nm, detwinning, exhibited by annihilation of  $\{112\}$  twin layers as a result of partial dislocations gliding on CTBs, is observed in both tension and compression; at higher strains, however,  $\{111\}$  incoherent twin boundaries, whose resistance to cracking contributes to strain hardening, are formed under tensile loading but not under compressive loading.

In recent years, nanotwinned metallic materials in face-centered cubic (FCC) systems have attracted intense research interest because of their superior strength compared with their twin-free counterparts.<sup>[1]</sup> Much effort is devoted to nanotwinned nanocrystalline metals, which exhibit simultaneous high ductility as a combined result of the dislocation nucleation from dislocation/grain boundary intersections and the dislocation gliding on

coherent twin boundaries (CTBs).<sup>[2]</sup> It is revealed that there exists a critical CTB spacing for which strength is maximized, similar to the optimal grain size in nanocrystals at the junction between the Hall-Petch effect and the inverse Hall-Petch effect.<sup>[3,4]</sup> On the other hand, nanotwinned small-sized metallic systems, for example, nanopillars and nanotubes, with either parallel or fivefold CTBs,<sup>[5]</sup> remain relatively lightly explored.<sup>[6]</sup> Compared with 3D nanocrystals, 1D nanopillars/nanotubes with free surfaces<sup>[7–9]</sup> attain additional geometric features including outer/inner diameter and cross-sectional shape which, along with the CTB spacing, may significantly alter their mechanical properties.<sup>[10–12]</sup> On the other hand, deformation may annihilate nanotwins and increase the CTB spacing.<sup>[13,14]</sup> These complicated processes and the underlying deformation mechanisms of nanopillars/nanotubes as a function of various characteristic sizes have not been fully understood.<sup>[15]</sup> Moreover, compared with the FCC lattice, nanotwinned metallic nanopillars in

body-centered cubic (BCC) systems are much less probed partly due to the more complicated plastic deformation mechanism in the latter.<sup>[16–18]</sup>


In the last two years, a few atomistic simulation studies have been dedicated to investigating deformation mechanisms of nanotwinned nanopillars<sup>[19,20]</sup> and nanotubes<sup>[21]</sup> in BCC metals. Sainath and Choudhary<sup>[19]</sup> discovered tension–compression asymmetric plastic deformation in nanotwinned Fe nanopillars, that is, twinning and dislocation slip in tension and compression, respectively; as a result, the tensile yield stress exhibits only marginal variation with respect to the CTB spacing, while the compressive yield stress increases with decreasing CTB spacing. In contrast, Xu et al.<sup>[20,21]</sup> reported that the plastic deformation of nanotwinned tungsten (W) nanopillars/nanotubes is dominated by dislocation slip in both tension and compression. Thus, a question arises regarding how the CTB spacing influences the uniaxial deformation of nanotwinned W nanopillars.

In this Letter, we examine tensile and compressive deformation mechanisms in nanotwinned W crystals and nanopillars with varying CTB spacing using molecular dynamics (MD) simulations. A nanotwinned crystal and a nanotwinned nanopillar containing  $\{112\}$  CTB with alternate crystallographic orientations  $x[110]$ ,  $y[1\bar{1}1]$ ,  $z[1\bar{1}2]$  and  $x[110]$ ,  $y[\bar{1}11]$ ,  $z[1\bar{1}2]$  in adjacent grains are shown in **Figure 1**. In the cube-shaped

Dr. S. Xu  
California NanoSystems Institute  
University of California  
Santa Barbara, CA 93106-6105, USA  
E-mail: shuozhixu@ucsb.edu

Dr. S. Z. Chavoshi  
Department of Mechanical Engineering  
Imperial College London  
London SW7 2AZ, UK

Dr. Y. Su  
Department of Mechanical Engineering  
University of California  
Santa Barbara, CA 93106-5070, USA

 The ORCID identification number(s) for the author(s) of this article can be found under <https://doi.org/10.1002/pssr.201700399>.

DOI: 10.1002/pssr.201700399

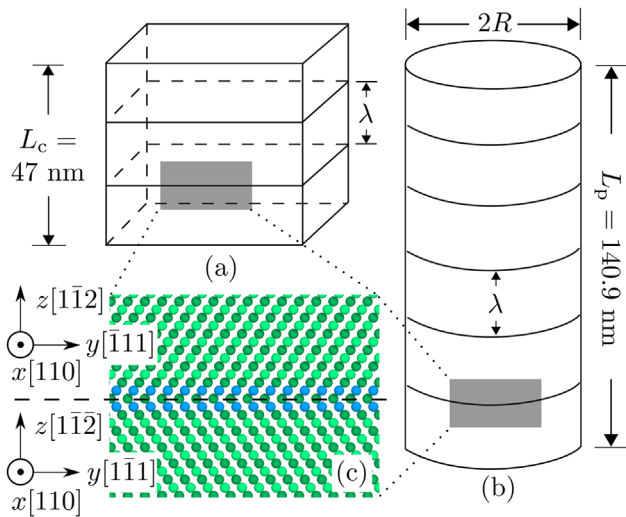


**Figure 1.** Atomistic structures of (a) a cube-shaped nanotwinned crystal with edge length  $L_c = 47$  nm and (b) a nanotwinned nanopillar with axial length  $L_p = 140.9$  nm and outer radius  $R = 20$  nm. Both the crystal and nanopillar have alternate crystallographic orientations in adjacent grains with a uniform CTB spacing  $\lambda$ . A close-up view of the CTB is presented in (c) with atoms colored by the coordination number.

crystals, periodic boundary conditions (PBCs) are applied along all three directions; in the nanopillars, PBCs are imposed on the  $z$  axis, with all other boundaries assumed traction-free. All crystals have the same edge length  $L_c = 47$  nm, with a uniform CTB spacing  $\lambda$  varying from 1 nm to 23.48 nm, while all nanopillars have the same axial length  $L_p = 140.9$  nm and outer radius  $R = 20$  nm, with  $\lambda$  varying from 1 to 70.45 nm. With a lattice parameter of 3.14339 Å, a crystal and a nanopillar has approximately 6.7 and 11.4 million atoms, respectively. Twin-free structures, including a single crystal and a single crystalline nanopillar, are also studied as references.

Each crystal/nanopillar is first dynamically relaxed for 20 ps at 10 K under an isobaric zero-stress condition, before the structure is energy minimized using the conjugate gradient method. It follows that a homogeneous deformation at a constant engineering strain rate of  $\pm 10^9$  s $^{-1}$  at a constant temperature of 10 K is applied along the  $z$  direction until the uniaxial engineering strain  $\epsilon$  reaches  $\pm 0.2$ , during which an NPT ensemble is employed in crystals to maintain zero transverse stresses in the  $x$ - $y$  plane, while an NVT ensemble is used in nanopillars.<sup>[22]</sup> In all dynamic simulations, a velocity Verlet algorithm is adopted with a time step of 2 fs; the uniaxial engineering stress  $\sigma$  is calculated following the virial stress formulation. All atomistic simulations are performed using LAMMPS.<sup>[23]</sup> The embedded atom method (EAM) potential of Marinica et al.,<sup>[24]</sup> which has been proven to well describe the deformation of W nanopillars/nanotubes,<sup>[20,21]</sup> is employed for the interactions between W atoms. Atomistic structures are visualized in OVITO<sup>[25]</sup> with lattice defects identified by the centrosymmetry parameter (CSP)<sup>[26]</sup> and adaptive common neighbor analysis (a-CNA).<sup>[27]</sup>

**Figure 2** presents the yield stress  $\sigma_Y$ , which corresponds to defects initiation, as a function of the CTB spacing  $\lambda$ , in cases of

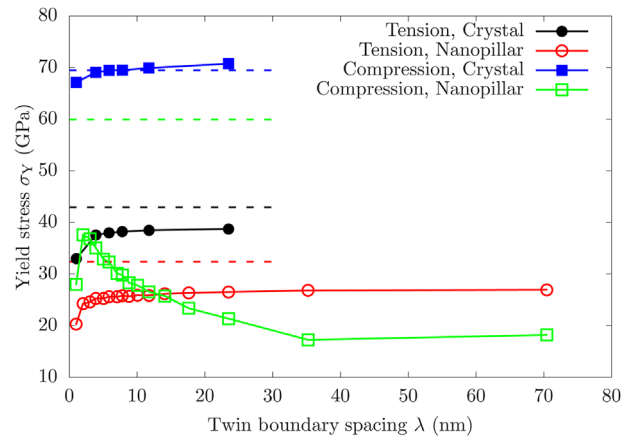


**Figure 2.** Yield stress  $\sigma_Y$  as a function of the CTB spacing  $\lambda$  for nanotwinned crystals and nanotwinned nanopillars under tensile and compressive loading. Horizontal dashed lines are the yield stresses of the single crystal and the single crystalline nanopillar, distinguished by color.

nanotwinned crystals and nanotwinned nanopillars under tensile and compressive loading; values of  $\sigma_Y$  for the single crystal and single crystalline nanopillar are also plotted as references. It is shown that (i) for the same  $\lambda$ , the nanotwinned nanopillars have a lower  $\sigma_Y$  than the nanotwinned crystals; (ii)  $\sigma_Y$  of the nanotwinned structures are close to or lower than their single crystalline counterparts; (iii)  $\sigma_Y$  of the nanotwinned crystals in both tension and compression is almost independent of  $\lambda$ , except that the smallest  $\lambda$  of 1 nm is accompanied by a lower  $\sigma_Y$ ; and (iv) for the nanotwinned nanopillars,  $\sigma_Y$  is almost invariant with respect to  $\lambda$  (except a lower  $\sigma_Y$  for  $\lambda = 1$  nm) under tensile loading, while it varies more significantly with  $\lambda$  under compressive loading, with the maximum  $\sigma_Y$  achieved at  $\lambda = 2.01$  nm.

Results (i) and (ii) above can be attributed to the existence of free surfaces and CTBs, which serve as dislocation sources, in nanopillars and nanotwinned structures, respectively. The other two results, however, are not straightforward to explain. To correlate the stress-strain response with underlying deformation mechanisms, we analyze the atomistic structures. First, a common factor in results (iii) and (iv) is the peculiarity of the case of  $\lambda = 1$  nm. A closer look at the atomistic structures discovers that kink-like steps are formed along CTBs after dynamic relaxation, i.e., prior to loading, as shown in **Figure 3**. Chen and Kulkarni<sup>[28]</sup> found that the attractive entropic interactions between adjacent CTBs, which scale with  $1/\lambda^2$ , enhance the CTBs' thermal fluctuations which then change their local structures. Specifically for the nanotwinned crystals, on the threshold of yielding, atoms in the vicinity of the CTBs undergo phase transformation from the BCC to the FCC and the hexagonal close-packed (HCP) structures under tensile and compressive loading, respectively,<sup>[20]</sup> which is the case for all  $\lambda$ . Since the kinked CTBs are more susceptible to defect nucleation,<sup>[29]</sup> the corresponding yield stress drops. These findings justify result (iii).

In the nanotwinned nanopillars, when  $\lambda \geq 2$  nm, yielding is controlled by distant and adjacent dislocation nucleation from free surface/CTB intersections in tension and compression,

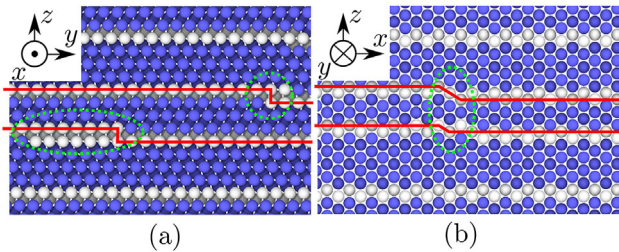


**Figure 3.** Projections of the atomistic structure of the nanotwinned crystal with  $\lambda = 1$  nm on (a) the  $\gamma$ - $z$  plane and (b) the  $x$ - $z$  plane after dynamic relaxation but prior to loading. CTBs are shown along red solid lines with kink-like steps indicated by dotted green circles. Atoms are colored by a-CNA<sup>[27]</sup>: blue are coordinated as BCC and white are of unknown local structure.

respectively, in agreement with the uniaxial deformation of nanotwinned nanotubes with  $\lambda \geq 3.06$  nm.<sup>[21]</sup> These dislocations then glide on  $\{110\}$  slip planes and interact with CTBs, as shown in **Figure 4(a)**. Prior MD simulations in W found that CTBs are weak barriers to single lattice dislocation,<sup>[30,31]</sup> but strong barriers to successive lattice dislocations on adjacent slip planes.<sup>[21]</sup> As a result, when  $\lambda \geq 2$  nm, the yield stress  $\sigma_Y$  increases with a smaller  $\lambda$  under compressive loading while is almost constant with different  $\lambda$  under tensile loading. When  $\lambda > 15$  nm, for the same  $\lambda$ , the compressive yield stress is lower than the tensile yield stress in the nanopillars, in contrast to that in the crystals. This phenomenon may be related to prior experiments in W which revealed a critical pillar diameter of about 500 nm above which the compressive yield stress is higher while below which the tensile yield stress is higher.<sup>[32]</sup>

When  $\lambda = 1$  nm, in the absence of  $\{110\}$  dislocations, CTBs near the free surface become inclined, then successive  $\{112\}$  CTB partial dislocations are nucleated from surface/CTB intersections, gliding along and merging CTBs, exhibited as the early stage of detwinning, as shown in **Figure 4(b)** and **Figure 5(a)**. It is the resolved shear stress on the locally inclined CTBs that provides the driving force for partial dislocation nucleation and gliding. We remark that similar phenomenon does not take place during the uniaxial deformation of the nanotwinned crystals, suggesting that it is indeed the  $\{112\}$  CTB partial dislocations but not the attractive entropic interactions between adjacent CTBs that plays an important role in the detwinning process in the nanotwinned nanopillars.

Under tensile loading, the detwinning propagates toward the nanopillar center, leaving behind incoherent twin boundaries (ITB) on  $\{111\}$  planes, as shown in **Figure 4(c-d)**. For all  $\lambda$ , the nanopillars eventually break by a crack formed on  $\{112\}$  planes: when  $\lambda \geq 2$  nm, the crack propagates along CTBs, which are the preferential cracking sites<sup>[33]</sup>; when  $\lambda = 1$  nm, the growth of the  $\{112\}$  crack is impeded by  $\{111\}$  ITBs, which are known to have a high cracking resistance.<sup>[34]</sup> The crack/ITB interactions contribute to the strain hardening, which is observed only in the case of  $\lambda = 1$  nm among all nanopillars under tension (**Figure 4(e)**).

Under compressive loading, the detwinning proceeds at an increasing strain in the case of  $\lambda = 1$  nm, with the result that more twin layers are annihilated, as shown in **Figure 5(b)**, similar to the detwinning process in nanotwinned Cu

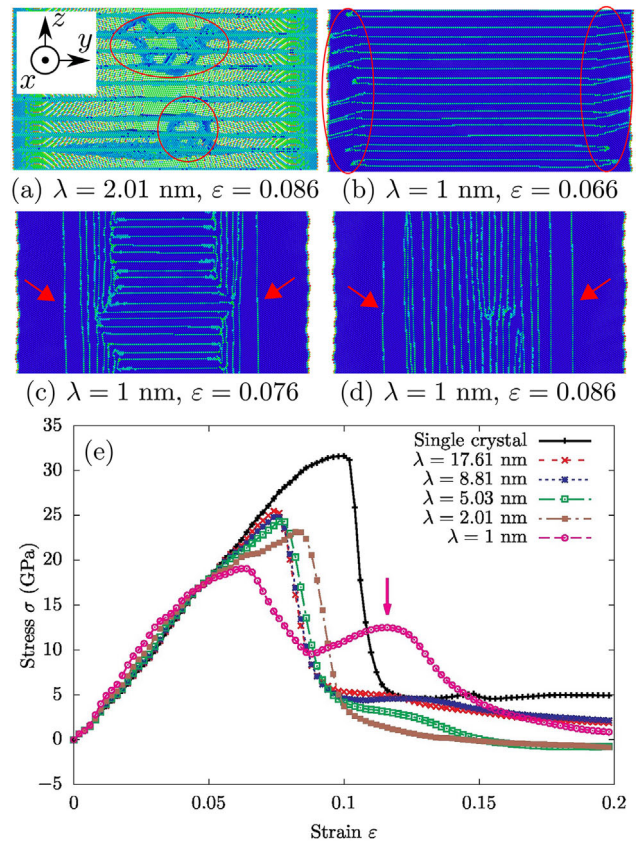


**Figure 4.** Atomistic structure of the nanotwinned nanopillars with (a)  $\lambda = 2.01$  nm and (b-d)  $\lambda = 1$  nm at different uniaxial engineering strain  $\epsilon$  under tensile loading. Atoms are colored by CSP<sup>[26]</sup> between 0 and 30; those with a CSP smaller than one are deleted in (a). In (a), dislocations, indicated by red circles and nucleated from free surface/CTB intersections, glide on distant  $\{110\}$  slip planes and interact with CTBs. In (b), successive  $\{112\}$  CTB partial dislocations are nucleated from surface/CTB intersections, gliding along and merging CTBs; the subsurface areas are highlighted by red circles. In (c-d),  $\{111\}$  ITBs (indicated by red arrows) are formed at higher strains. (e) Stress-strain curves for single crystalline and nanotwinned nanopillars with different  $\lambda$ : the case of  $\lambda = 1$  nm is the only one exhibiting strain hardening, indicated by the magenta arrow, as a result of the crack/ITB interactions.

nanopillars under torsional loading.<sup>[13]</sup> In contrast to tensile loading, no  $\{111\}$  ITBs are formed. With further compression, new dislocations start to nucleate from the free surface/CTB intersections, gliding on  $\{110\}$  planes and interacting with CTBs, as in the cases of larger  $\lambda$ . For  $\lambda = 1$  nm, the average CTB spacing increases to about 6 nm (would be 6.8 nm in the undeformed configuration given  $\epsilon = 0.12$ ) prior to dislocation/CTB interactions; consequently, its yield stress, 27.98 GPa, is close to that in the case of  $\lambda = 7.05$  nm, 30.12 GPa. Result (iv) is thus rationalized. Note that for all  $\lambda$ , (i) the nanopillars eventually fail by the formation of shear bands on  $\{110\}$  planes across the nanopillar cross section,<sup>[20,22]</sup> and (ii) the first peak on the stress-strain curves at  $\epsilon \approx 0.045$  is due to the homogeneous nucleation of twinning-like planar defects which were also found in single/nanotwinned crystals<sup>[20]</sup> and single crystalline/nanotwinned nanotubes,<sup>[21]</sup> in which case the yield stresses are taken at the

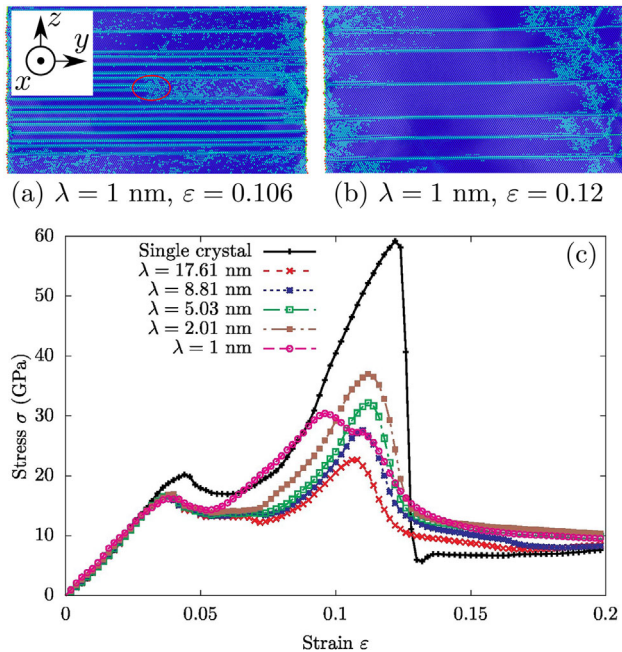


**Figure 5.** (a–b) Atomistic structure of the nanotwinned nanopillars with  $\lambda = 1$  nm at different uniaxial engineering strain  $\varepsilon$  under compressive loading. Atoms are colored by CSP<sup>[26]</sup> between 0 and 30. In (a), successive  $\{112\}$  CTB partial dislocations are nucleated from surface/CTB intersections, gliding along and merging CTBs; the edge of a twin layer is highlighted by the red circle. In (b), the detwinning process proceeds with more twin layers annihilated. (c) Stress–strain curves for single crystalline and nanotwinned nanopillars with different  $\lambda$ .

initiation of dislocations right before the second, that is, the highest, peak on the stress–strain curves.

It is instructive to compare the MD simulation results of the nanotwinned nanopillars in BCC metals with those in FCC metals. In experimental studies and MD simulations of nanotwinned nanopillars under tensile loading, as the CTB spacing  $\lambda$  decreases, Jang et al.<sup>[6]</sup> revealed a critical  $\lambda$  ( $\sim 3$ – $4$  nm) for brittle-to-ductile transition in Cu, while Wang et al.<sup>[35]</sup> observed a critical  $\lambda$  ( $= 2.8$  nm) for ductile-to-brittle transition in Au. This difference may be attributed to the intrinsically brittle and ductile nature of the CTB in Cu and Au, respectively,<sup>[36]</sup> and cannot be explained simply based on the CTB energy, which is very close between the two materials:  $22.2 \text{ mJ m}^{-2}$  in Cu with the Mishin EAM potential<sup>[37]</sup> and  $21.7 \text{ mJ m}^{-2}$  in Au with the Grochola EAM potential.<sup>[38]</sup> The finding that a small  $\lambda$  leads to unusual mechanical responses in nanotwinned FCC nanopillars echoes with the current work in BCC W, but in a different way: in our simulations, no ductile-to-brittle transition is observed with  $\lambda$  down to 1 nm; instead, detwinning occurs, resulting in  $\{111\}$  ITBs in tensile loading and a large CTB spacing in compressive loading. We note that, with  $\lambda$  decreasing to 2.8 nm, no transition in the deformation mechanism was reported in nanotwinned Fe nanopillars.<sup>[19]</sup> These observations highlight the complexity of the deformation mechanisms in nanotwinned metal nanopillars, which merit further investigations.

In conclusion, we report MD simulation results of the uniaxial deformation of nanotwinned W nanopillars with a varying CTB

spacing  $\lambda$ . Nanotwinned crystals with the same  $\lambda$ , a single crystal, and a single crystalline nanopillar, are also investigated for references. Our simulations reveal a novel tension–compression asymmetric deformation mechanisms, in conjunction with the effects of  $\lambda$ . Specifically, when  $\lambda \geq 2$  nm, the onset of plasticity is exhibited by the nucleation of dislocations from free surface/CTB intersections, gliding on distant and adjacent  $\{110\}$  slip planes under tensile and compressive loading, respectively. As a result, the tensile yield stress is almost invariant with respect to  $\lambda$ , while the compressive yield stress increases as  $\lambda$  becomes smaller. When  $\lambda$  reduces to 1 nm, however, CTB partial dislocations on  $\{112\}$  planes are nucleated from free surface/CTB intersections, moving adjacent CTBs close to each other and annihilating twin layers parallel to CTBs; as the strain increases further,  $\{111\}$  ITBs are formed and resistant cracking in tensile loading while the detwinning process continues on  $\{112\}$  planes in compressive loading. Consequently, in both tension and compression, the yield stress in the case of  $\lambda = 1$  nm is lower than that for some larger  $\lambda$ .

We remark that recently developed experimental techniques in growing nanoscale twins in FCC metals with high stacking fault energies<sup>[39]</sup> may open up avenues for manufacturing nanotwinned nanopillars in BCC metals, which hasn't been achieved to our best knowledge. In this regard, our work may serve as a precursor to encourage more computational and experimental work in this topic.

## Acknowledgements

We thank Dr. Dengke Chen and Mr. Thomas G. Payne for helpful discussions. The work of SX was supported in part by the Elings Prize Fellowship in Science offered by the California NanoSystems Institute (CNSI) on the UC Santa Barbara campus. SX also acknowledges support from the Center for Scientific Computing from the CNSI, MRL: an NSF MRSEC (DMR-1121053). SZC would like to express his sincere gratitude for the financial support from the AVIC Center for Materials Characterization, Processing, and Modeling at Imperial College London. This work used the Extreme Science and Engineering Discovery Environment (XSEDE), which is supported by National Science Foundation grant number ACI-1053575.

## Conflict of Interest

The authors declare no conflict of interest.

## Keywords

coherent twin boundaries, molecular dynamics, nanopillars, nanotwinned materials, tungsten

Received: November 23, 2017  
Revised: December 22, 2017  
Published online: January 19, 2018

- [1] L. Lu, Y. Shen, X. Chen, L. Qian, K. Lu, *Science* **2004**, 304, 422.
- [2] K. Lu, L. Lu, S. Suresh, *Science* **2009**, 324, 349.
- [3] L. Lu, X. Chen, X. Huang, K. Lu, *Science* **2009**, 323, 607.

- [4] X. Li, Y. Wei, L. Lu, K. Lu, H. Gao, *Nature* **2010**, 464, 877.
- [5] X. Zhang, X. Li, H. Gao, *Acta Mech. Sin.* **2017**, 33, 792.
- [6] D. Jang, X. Li, H. Gao, J. R. Greer, *Nature Nanotechnol.* **2012**, 7, 594.
- [7] S. Z. Xu, Z. M. Hao, Q. Wan, *IOP Conf. Ser.: Mater. Sci. Eng.* **2010**, 10, 012175.
- [8] Y. Su, S. Xu, *Mater. Sci. Eng. A* **2016**, 678, 153.
- [9] S. Xu, Y. Su, D. Chen, L. Li, *Mater. Lett.* **2017**, 193, 283.
- [10] Y. Zhang, H. Huang, *Nanoscale Res. Lett.* **2008**, 4, 34.
- [11] C. Deng, F. Sansoz, *Appl. Phys. Lett.* **2009**, 95, 091914.
- [12] F. Hammami, Y. Kulkarni, *J. Appl. Phys.* **2014**, 116, 033512.
- [13] H. Zhou, X. Li, Y. Wang, Z. Liu, W. Yang, H. Gao, *Nano Lett.* **2015**, 15, 6082.
- [14] G. Cheng, S. Yin, T. H. Chang, G. Richter, H. Gao, Y. Zhu, *Phys. Rev. Lett.* **2017**, 119, 256101.
- [15] J. R. Greer, J. T. M. De Hosson, *Prog. Mater. Sci.* **2011**, 56, 654.
- [16] S. Z. Xu, Z. M. Hao, Y. Q. Su, Y. Yu, Q. Wan, W. J. Hu, *Comput. Mater. Sci.* **2011**, 50, 2411.
- [17] S. Z. Xu, Z. M. Hao, Y. Q. Su, W. J. Hu, Y. Yu, Q. Wan, *Radiat. Eff. Defects Solids* **2012**, 167, 12.
- [18] S. Xu, Y. Su, *Modelling Simul. Mater. Sci. Eng.* **2016**, 24, 085015.
- [19] G. Sainath, B. K. Choudhary, *Philos. Mag.* **2016**, 96, 3502.
- [20] S. Xu, J. K. Startt, T. G. Payne, C. S. Deo, D. L. McDowell, *J. Appl. Phys.* **2017**, 121, 175101.
- [21] S. Xu, S. Z. Chavoshi, *Curr. Appl. Phys.* **2018**, 18, 114.
- [22] S. Xu, Y. Su, D. Chen, L. Li, *Appl. Phys. A* **2017**, 123, 788.
- [23] S. Plimpton, *J. Comput. Phys.* **1995**, 117, 1.
- [24] M. C. Marinica, L. Ventelon, M. R. Gilbert, L. Proville, S. L. Dudarev, J. Marian, G. Bencteux, F. Willaime, *J. Phys.: Condens. Matter* **2013**, 25, 395502.
- [25] A. Stukowski, *Modell. Simul. Mater. Sci. Eng.* **2010**, 18, 015012.
- [26] C. L. Kelchner, S. J. Plimpton, J. C. Hamilton, *Phys. Rev. B* **1998**, 58, 11085.
- [27] A. Stukowski, *Modell. Simul. Mater. Sci. Eng.* **2012**, 20, 045021.
- [28] D. Chen, Y. Kulkarni, *J. Mech. Phys. Solids* **2015**, 84, 59.
- [29] Y. M. Wang, F. Sansoz, T. LaGrange, R. T. Ott, J. Marian, T. W. Barbee, Jr, A. V. Hamza, *Nature Mater.* **2013**, 12, 697.
- [30] Y. Cheng, M. Mrovec, P. Gumbsch, *Philos. Mag.* **2008**, 88, 547.
- [31] M. Mrovec, C. Elsässer, P. Gumbsch, *Philos. Mag.* **2009**, 89, 3179.
- [32] J. Y. Kim, D. Jang, J. R. Greer, *Acta Mater.* **2010**, 58, 2355.
- [33] L. Li, Z. Zhang, P. Zhang, Z. Zhang, *Scr. Mater.* **2011**, 65, 505.
- [34] L. L. Li, P. Zhang, Z. J. Zhang, Z. F. Zhang, *Sci. Rep.* **2014**, 4, 3744.
- [35] J. Wang, F. Sansoz, J. Huang, Y. Liu, S. Sun, Z. Zhang, S. X. Mao, *Nature Commun.* **2013**, 4, 1742.
- [36] L. Pei, C. Lu, K. Tieu, X. Zhao, L. Zhang, K. Cheng, G. Michal, *Mater. Lett.* **2015**, 152, 65.
- [37] Y. Mishin, M. J. Mehl, D. A. Papaconstantopoulos, A. F. Voter, J. D. Kress, *Phys. Rev. B* **2001**, 63, 224106.
- [38] G. Grochola, S. P. Russo, I. K. Snook, *J. Chem. Phys.* **2005**, 123, 204719.
- [39] D. Bufford, Y. Liu, Y. Zhu, Z. Bi, Q. X. Jia, H. Wang, X. Zhang, *Mater. Res. Lett.* **2013**, 1, 51.